Royal Netherlands Institute for Sea Research

This is a postprint of:

Lønborg, C., Yokokawa, T., Herndl, G.J. & Alvarez-Salgado, X.A. (2015). Production and degradation of fluorescent dissolved organic matter in surface waters of the eastern north Atlantic ocean. Deep Sea Research, Part A. Oceanographic Research Papers, 96, 28–37

Published version: dx.doi.org/10.1016/j.dsr.2014.11.001

Link NIOZ Repository: www.vliz.be/nl/imis?module=ref&refid=

[Article begins on next page]

The NIOZ Repository gives free access to the digital collection of the work of the Royal Netherlands Institute for Sea Research. This archive is managed according to the principles of the Open Access Movement, and the Open Archive Initiative. Each publication should be cited to its original source - please use the reference as presented.
When using parts of, or whole publications in your own work, permission from the author(s) or copyright holder(s) is always needed.

1 Production and degradation of fluorescent dissolved organic matter in surface waters of the
2 eastern North Atlantic Ocean

3 Christian Lønborg[a,b*], Taichi Yokokawa[c], Gerhard J. Herndl[d,e] and Xosé Antón Álvarez-
4 Salgado[a]

5 [a] IIM–CSIC, Instituto de Investigacións Mariñas, Eduardo Cabello 6, 36208 Vigo, Spain
6 [b] Australian Institute of Marine Science, PMB 3, Townsville MC, QLD 4810, Australia
7 [c]Center for Marine Environmental Studies, Ehime University, Matsuyama 790–8577, Japan
8 [d] Department of Limnology and Oceanography, University of Vienna, Althanstrasse 14
9 A-1090 Vienna, Austria.
10 [e]Department of Biological Oceanography, Royal Netherlands Institute for Sea Research
11 (NIOZ), P.O. Box 59, 1790 AB Den Burg Netherlands.
12
13 [*]Corresponding author:
14 Australian Institute of Marine Science
15 PMB 3, Townsville MC, QLD 4810
16 Australia
17 Phone: 0061 (0) 7 4753 4382
18 Fax: 0061 (0) 7 4772 5852
19 Email: clonborg@gmail.com

20 **Abstract**

21 The distribution and fate of coloured dissolved organic matter (CDOM) in the epipelagic
22 Eastern North Atlantic was investigated during a cruise in the summer 2009 by combining
23 field observations and culture experiments. Dissolved organic carbon (DOC) and nitrogen
24 (DON), the absorption spectra of CDOM and the fluorescence intensity of proteins (Ex/Em
25 280/320 nm; *F*(280/320)) and marine humic-like substances (*F*(320/410)) were measured in
26 the upper 200 m. DOC and DON showed higher concentrations in the top 20 m than below,
27 and DOC increased southwards, while DON decreased. *F*(280/320) and *F*(320/410) showed
28 maxima near the deep chlorophyll maximum (at about 50 m), suggesting that these
29 fluorophores were linked to phytoplankton production and the metabolism of the associated
30 microbial community. The coloured and fluorescent fractions of DOM showed low levels
31 south of the Azores Front, at about 35°N, likely due to the accumulated photobleaching of
32 the waters transported eastwards by the Azores current into the study area (at 20ºW).
33 Twelve culture experiments were also conducted with surface water (5 m) to assess the
34 impact of microbial degradation processes on the bulk, coloured and fluorescent fractions
35 of DOM. After 72 hours of incubation in the darkness, 14 ± 9% (average ± SD) of the
36 initial DON was consumed at an average rate of 0.24 ± 0.14 µmol l^{-1} d^{-1} and the protein-
37 like fluorescence decayed by 29 ± 9% at a net rate of 0.06 ± 0.03 QSU d^{-1}. These rates
38 were significantly lower south of the Azores front, suggesting that DOM in this region was
39 of a more recalcitrant nature. Conversely, the marine humic-like fluorescence increased at a
40 net rate of 0.013 ± 0.003 QSU d^{-1}. The close linear relationship of DON uptake with
41 *F*(280/320) consumption (R^2= 0.91, p <0.0001, n = 12) and *F*(320/410) production (R^2=
42 0.52, p <0.008, n = 12) that we found during these incubation experiments suggest that the
43 protein-like fluorescence can be used as a proxy for the dynamics of the labile DON pool

44 and that marine humic-like materials can be produced as a by-product of microbial DOM

45 degradation.

46 Keywords: Coloured dissolved organic matter, bioavailability, absorption and fluorescence

47 spectroscopy, Eastern North Atlantic Ocean.

48 **1. Introduction**

49 The largest pool of reactive nitrogen in the open ocean is contained in dissolved organic
50 matter (DOM), which originates mainly from phytoplankton and heterotrophic bacteria
51 exudation, viral cell lysis, protozoan grazing and zooplankton sloppy feeding (Bronk, 2002;
52 Nagata, 2000). Although a variable fraction of the DOM pool can be utilized by marine
53 microbes in hours to days, most of it is recalcitrant to microbial degradation over time-
54 scales of years to millennia (Hansell, 2013). In the coastal ocean, 22 ± 12 % (average ± SD
55 of an extensive global data base) of the dissolved organic carbon (DOC) and 35 ± 13 % of
56 the dissolved organic nitrogen (DON) is bioavailable with half-life times of 10 and 6 days,
57 respectively (Lønborg and Álvarez-Salgado, 2012). Information about the bioavailability
58 and degradation rates of DOM in open ocean waters is noticeably rarer, particularly in the
59 case of DON, but see the studies by Kirchman et al. (1991) and Lestcher et al. (2013) for
60 the few existing estimates (data range < 3 to 48%).

61 A fraction of the DOM pool absorbs light strongly in the UV and blue range of the
62 spectrum, with a part of this energy being re-emitted as fluorescence (Coble, 2007;
63 Stedmon and Álvarez-Salgado, 2011). This coloured DOM (CDOM) is a major factor
64 determining the underwater light field and attenuation of UV radiation in the ocean (Nelson
65 and Siegel, 2013). The fluorescence emission of CDOM (FDOM) in natural waters is
66 mainly due to protein- and humic-like compounds (Coble, 1996). The protein-like
67 fluorescence is related to the aromatic amino acids (tyrosine, tryptophan and
68 phenylalanine) and has been suggested as a suitable tracer for bio-labile DOM (Yamashita
69 and Tanoue, 2003; Lønborg et al., 2010). Conversely, the resistance to microbial
70 degradation of humic materials has led to consider the humic-like fluorescence as an
71 indicator for recalcitrant DOM, which is either of terrestrial origin or generated as a by-

72 product of the microbial degradation of biogenic organic matter (Nieto-Cid et al., 2006;
73 Yamashita and Tanoue, 2008; Lønborg et al., 2010; Jørgensen et al., 2011, Kowalczuk et
74 al., 2013). Andrew et al. (2013) has also suggested that chemical or microbial modification
75 of terrestrial organic material could also be an alternative source of humic-like FDOM.
76 Although numerous studies have used the fluorescence intensity of protein- and humic-like
77 compounds to trace changes in the composition, production and degradation of DOM (e.g.
78 Coble et al., 1990; Guillemette and Del Giorgio, 2012), quantitative relationships between
79 DOM and FDOM properties are still lacking.

80 In this study we determined the distribution and fate of CDOM during a summer cruise
81 in the Eastern North Atlantic (ENA) Ocean from 42º to 27ºN by combining field
82 observations and culture experiments. This study is complementing the work by Lønborg
83 and Álvarez-Salgado (2014), who studied the variability of DOM and CDOM in the dark
84 ENA Ocean and Benavides et al. (2013) who studied the role of N_2 fixation and the uptake
85 and regeneration of DON in the upper water column during the same cruise. In this paper
86 we aimed at 1) describing the spatial variability of bulk, coloured and fluorescent DOM
87 components in epipelagic waters (0–200 m); 2) determining the short-term changes in
88 CDOM optical properties during seawater culture experiments; and 3) establishing
89 quantitative relationships between changes in FDOM and DOM bioavailability in the
90 epipelagic ENA Ocean.

91 2. Material and methods

92 *2.1. Field data*

93 Surface water samples (0–200 m) were collected during the CAIBOX cruise on board
94 the R/V *Sarmiento de Gamboa* from 25 July to 14 August 2009 (Fig. 1). Salinity,

95 temperature, chlorophyll *a* (Chl *a*), and inorganic nutrient (Nitrate-NO_3^-, Phosphate-

96 HPO_4^{2-} and Silicate- SiO_4H_4) profiles were obtained at 71 stations (white dots in Fig. 1).

97 Salinity, temperature and fluorescence of Chl *a* (F-Chl *a*) were recorded with a CTD

98 SeaBird 911 and a Sea-Tech fluorometer mounted on a General Oceanics rosette sampler

99 equipped with 24 Niskin bottles of 12 litres. Bottle samples were typically collected at 3- 4

100 depths ranging between 5 and 200 m. The CTD salinities were calibrated with bottle

101 samples analysed on board with a Guildline 8410-A Portasal. The F-Chl *a* records were

102 calibrated by filtration of 250 ml of sample water through a Whatman GF/F filter,

103 extraction in acetone (90% v/v), and fluorimetric determination with a Turner Designs

104 10000R fluorometer standardised with pure Chl *a* (Sigma) (Yentsch and Menzel, 1963).

105 Water samples for the analysis of inorganic nutrients were collected in 50 ml acid washed

106 polyethylene bottles and preserved in the dark at 4ºC until analysed on board within a few

107 hours.

108 The squared Brunt-Väisälä frequency (N^2) is commonly used to quantify the

109 stratification of the water column. Following Millard et al., (1990), N^2 can be calculated as:

110 $$N^2 = -\frac{g}{\rho} \cdot \frac{\partial \rho}{\partial z} = -g \cdot \frac{\partial \ln(\rho)}{\partial z} \qquad (1)$$

111 Where g is the gravity acceleration constant (9.8 m s^{-2}), z is the water depth, and ρ is the

112 water density at depth z. Integration of Eq. 1 between two depth levels (1 and 2),

113 $\overline{N}^2 = -g \cdot \ln(\rho_2/\rho_1)/(z_2 - z_1)$, provides a measure of the average stability of the water

114 column between z_1 and z_2. Here we will report values of $\overline{N}$, i.e., the square root of $\overline{N}^2$, in

115 min^{-1}. The higher the $\overline{N}$, the larger the stratification.

116 Profiles of dissolved organic carbon (DOC) and nitrogen (DON), absorption spectra of
117 coloured DOM (CDOM) and fluorescence intensities of protein- and humic-like substances
118 were obtained at 16 stations (black dots in Fig. 1).

119 *2.2. Incubation experiments*

120 Additional water was collected at 5 m at the first 12 of the 16 stations where DOM
121 variables were measured (framed stations in Fig. 1). This water was used to conduct
122 incubation experiments to measure changes in bulk concentrations and optical properties of
123 DOM over a period of 72 hours. Filtration of the water started within 20 min of collection;
124 one part was filtered through a dual-stage (0.8 µm and 0.2 µm) filter cartridge (Pall-
125 Acropak supor Membrane) which had been pre-washed with 10 l of Milli-Q water; the
126 second part was filtered through pre-combusted (450°C for 4 h) Whatman GF/C filters to
127 establish a microbial inoculum. After filtration, the water was transferred into a 20 l carboy
128 and the microbial inoculum was added to the 0.2 µm filtrate corresponding to 10% of the
129 total volume. Thereafter, the water was transferred into 20 glass bottles of 500 ml
130 (headspace ~100 ml), with four replicate bottles being sacrificed for analyses at times 0, 12,
131 24, 36 and 72 hours. The incubators were kept in the dark at 15°C, this temperature was
132 chosen as it represents the yearly average water temperature in the top 200 m in our study
133 area. Unfiltered water from these bottles was used at time 0 and 72 hours to follow changes
134 in bacterial production (BP). Samples for the analysis of dissolved inorganic nitrogen
135 (NH_4^+ and NO_3^-+NO_2^-) and phosphate (HPO_4^{2-}), DOC, total dissolved nitrogen (TDN) and
136 CDOM absorption were collected in four replicates at 0 and 72 hours. DOM fluorescence
137 (FDOM) was measured at all time points. The samples for the dissolved phase were
138 collected after filtration through 0.2 µm filters (Pall Supor membrane Disc) in an acid-

139 cleaned glass filtration system under low N_2 flow pressure. Water samples for inorganic

140 nutrients (NH_4^+, NO_3^-+NO_2^- and HPO_4^{2-}) were collected in 50 ml acid washed (HCl)

141 polyethylene bottles and kept frozen (-20°C) until measured in the base laboratory. All

142 glasswares used were first acid-washed in 10% HCl and thereafter rinsed with Milli-Q and

143 sample water prior to use.

144 *2.3. Sample measurements*

145 BP was determined by [^{3}H]-leucine incorporation as outlined in Yokokawa et al. (2012).

146 Briefly, duplicate subsamples (1.5 ml) were dispensed into screw capped 2.0 ml centrifuge

147 tubes and 5 nM (final concentration) of [^{3}H]-leucine was added and incubated at 15°C in

148 the dark for 1 to 4 h. One trichloroacetic acid (TCA)-killed blank was used per sample. The

149 incubation was terminated by adding TCA (final concentration 5%), and the samples were

150 centrifuged at 18,000 × g for 10 min, followed by a TCA rinse (5%) and an ethanol rinse

151 (80%). Thereafter, 1.5 ml of scintillation cocktail (Ultima Gold) was added to the samples

152 and after 12-18 hours, the disintegrations per minute (DPM) were measured using a spectral

153 liquid scintillation counter (Perkin Elmer, Tri-Carb 3100TR). Quenching was corrected

154 using an external standard channel ratio and the DPM of the TCA-killed blank were

155 subtracted from the average DPM of the samples. The leucine incorporation rates were

156 expressed in pmol l^{-1} d^{-1}.

157 Inorganic nutrients (NH_4^+, NO_3^-+ NO_2^-, HPO_4^{2-} and SiO_4H_4) were determined using

158 standard segmented flow analysis (SFA) (Hansen and Koroleff, 1999). The precisions were

159 ± 0.05 μmol l^{-1} for NH_4^+ and SiO_4H_4, ± 0.1 μmol l^{-1} for NO_3^- + NO_2^- and ± 0.02 μmol l^{-1}

160 for HPO_4^{2-}.

161 Samples (10 ml) for DOC and TDN analysis were collected in pre-combusted (450ºC for
162 12 h) glass ampoules and preserved by adding 50 µl of 25 % H_3PO_4. DOC and TDN
163 samples were analysed using a Shimadzu total organic carbon analyser (platinum catalyst)
164 connected to an Antek TN measuring unit. Concentrations were determined by subtracting
165 a Milli-Q blank and dividing by the slope of a daily 4 points standard curve made from
166 potassium hydrogen phthalate and glycine. To avoid the small error associated with day-to-
167 day instrument variability, all samples from a given experiment were analysed on a single
168 day. Using the deep ocean reference samples (Batch 9–2009, Florida Strait at 700 m) we
169 obtained a concentration of 45.0 ± 1.4 µM for DOC and 33.4 ± 0.6 µM for TDN (average ±
170 SD, n = 6). The nominal values provided by the reference laboratory (Hansell laboratory)
171 are 41–44 and 32.25–33.75 µM, respectively. DON concentrations were calculated as the
172 difference between TDN and DIN (DON = TDN – DIN) with the standard error (SE)
173 calculated as the sum of the contributions: $SE^2_{DON} = SE^2_{TDN} + SE^2_{NH4} + SE^2_{NO3+NO2}$. The
174 DOM consumed over the 72 hours incubation is defined here as the bioavailable pool
175 (BDOM), and the remaining as the resistant pool (RDOM). The DOM utilization rate was
176 calculated by dividing BDOM by the incubation time (BDOM/Δt).
177 The CDOM absorption spectra were measured on a Perkin Elmer Lambda 950
178 spectrophotometer equipped with 10 cm quartz cells using Milli-Q water as a blank.
179 Spectral scans were collected between 250 and 750 nm. The absorption coefficient at any
180 wavelength, $a_{CDOM}(\lambda)$ (m^{-1}), was calculated as:

$$a_{CDOM}(\lambda) = 23.03 \times [Abs(\lambda) - Abs(600\text{–}750)] \quad (2)$$

181 Where Abs(λ) is the absorbance at wavelength λ, and Abs(600–750) is the average
182 absorbance between 600 and 750 nm, which corrects for the residual scattering by fine size

183 particle fractions, micro-air bubbles or colloidal material present in the sample, or refractive
184 index differences between the sample and the reference (m^{-1}), the factor 23.03 converts
185 from decadic to natural logarithms and furthermore considers the cell path-length. The
186 estimated detection limit of this spectrophotometer is 0.001 absorbance units or $0.02 m^{-1}$.
187 CDOM fluorescence was measured using a Perkin Elmer LS 55 luminescence
188 spectrometer working with a xenon discharge lamp, equivalent to 20 kW for 8 μs duration,
189 and a 1-cm quartz fluorescence cell. The slit width was 10.0 nm for the excitation and
190 emission wavelengths and an integration time 60 seconds was used. Measurements were
191 performed at a constant temperature of 20°C and Milli-Q water was used as a blank. The
192 excitation/emission (Ex/Em) point measurements were performed at the traditional humic-
193 like peaks A (average Ex/Em, 250/435 nm; termed *F*(250/435)), C (terrestrial humic-like
194 substances, average Ex/Em wavelengths of 340/440 nm; termed *F*(340/440)), M (marine
195 humic-like substances, average Ex/Em, 320/410 nm; termed *F*(320/410)) and the protein
196 peak T (protein-like substances, average Ex/Em, 280/320 nm; termed *F*(280/320)) as
197 proposed by Coble (1996). Fluorescence measurements were expressed in quinine sulphate
198 units (QSU), i.e., in μg equivalents of QS l^{-1}, by calibrating at Ex/Em 350/450 nm against a
199 quinine sulphate dihydrate (QS) standard dissolved in 0.05 M sulphuric acid. The limit of
200 detection limit, calculated as 3 × the standard deviation of the blank, was 0.03 QSU for
201 *F*(250/435), 0.05 QSU for *F*(340/440) and 0.02 QSU for *F*(320/410) and *F*(280/320).
202 Whereas *F*(250/435) and *F*(340/440) did not change significantly during the course of the
203 experiments (see results section), *F*(280/320) decayed and *F*(320/410) built-up according to
204 a first-order kinetics (Fig. 2). The *F*(280/320) consumed over the 72 hours incubation was
205 here defined as the bioavailable pool (B*F*(280/320)), and the remaining as the resistant
206 fraction (R*F*(280/320)). The *F*(280/320) utilization rate was calculated by dividing

207 B*F*(280/320) by the incubation time (B*F*(280/320)/Δt). The built-up of *F*(320/410) over the

208 incubation period is defined as the produced pool (P*F*(320/410)), and the remaining at the

209 end of the incubation as the resistant fraction (R*F*(320/410)).

210 Single linear regression analyses were performed to obtain the best-fitting coefficients

211 between pairs of variables obtained with regression model II as described in Sokal and

212 Rohlf (1995). Prior to regression, normality was checked and the confidence level was set

213 at 95%, with all statistical analysis conducted in Statistica 6.0. The coefficient of variation

214 (C.V.) was calculated as the (Standard deviation/Mean) × 100.

215

216 **3. Results**

217 *3.1. Hydrographic and chemical characteristics of the surface Eastern North Atlantic*

218 *(ENA) ocean*

219 Salinity varied between 35.3 and 37.2, increasing westwards (from the coast to the open

220 ocean) and southwards (from the temperate to the subtropical ENA) with the presence of a

221 sharp salinity gradient at about 35°N (see the meridional evolution of the depth of the 36.2

222 isohaline; Fig. 3a). The temperature varied between 12.5 and 24.9°C, increasing westwards

223 and southward with an abrupt gradient again at 35ºN (see the meridional evolution of the

224 depth of the 16.2ºC isotherm; Fig. 3b). A marked seasonal thermocline was detected

225 between 50 and 70 m, which deepened southwards. These sharp salinity and temperature

226 gradients at about 35°N identify the position of the Azores front (Fig 3a and b). At the

227 stations close to the Canary Islands, the influence of the coastal upwelling of NW Africa

228 could be identified with more saline and colder water reaching shallower parts of the water

229 column (Fig. 3a & b).

230 The profiles of the Brunt-Väisälä frequency ($\overline{N}$) showed a marked stability maximum,
231 coinciding with the seasonal thermocline, throughout the cruise track (Fig. 3c). The profiles
232 south of 35°N showed slight increases of $\overline{N}$ between 50–100 m suggesting a higher degree
233 of stratification in this depth range (Fig. 3c). The Chl *a* profiles were characterised by
234 generally low values which varied between 0.10 and 1.69 mg m^{-3}, with higher
235 concentrations north of 35°N (Fig. 3d). The high stability of the water column at around 50
236 m favoured the development of a marked deep chlorophyll maxima (DCM) to the north of
237 35ºN, which weakened dramatically and deepened down to approx. 100 m south of that
238 position (Fig. 3d). The DCM became shallower close to the Canary Islands in response to
239 coastal upwelling.
240 Inorganic nutrient concentrations were generally around the detection limit in the upper
241 50 m (Fig. 3e & f). In parallel to the meridional change of water temperature below the
242 seasonal thermocline, subsurface nutrient levels were higher north of 35°N, while they were
243 around the detection limit down to 200 m south of that latitude. The influence of the NW
244 African upwelling area could be detected at the southern stations with nutrients (> 3 µM for
245 NO_3^- and > 0.15 µM for HPO_4^{2-}) reaching shallower parts of the water column (Fig. 3e &
246 f).
247 Higher levels of DOC and DON were generally observed in the surface 50 m with
248 average ± SD concentrations of 66 ± 7 µmol l^{-1} of C and 6.3 ± 0.9 µmol l^{-1} of N, and
249 decreasing towards average values of 54 ± 3 µmol l^{-1} of C and 5.6 ± 0.4 µmol l^{-1} of N at
250 200 m (Fig. 4a & b). DOC concentrations increased southwards while DON decreased,
251 resulting in an increasing average C/N ratio of DOM from 10 to 12 in the surface 50 m
252 (Fig. 4a, b & c). The upwelling of NW Africa was detectable at the southernmost stations

253 with more DOC-depleted deep water reaching the surface, while no clear impact was found
254 for DON (Fig. 4a, b & c). The average ± SD C/N molar ratio of the upper 50 m, 11 ± 2, was
255 not significantly different form the C/N molar ratio at 200 m, 10 ± 2.

256 The CDOM absorption and fluorescence indices used in this work varied similarly with
257 position and depth (Fig. 4d-g). Absorption coefficients at 254 nm ($a_{CDOM}(254)$) and 340 nm
258 ($a_{CDOM}(340)$) and fluorescence intensities of protein-like ($F(280/320)$) and marine humic-
259 like ($F(320/410)$) substances were generally higher near the coast than in the open ocean
260 and decreased southwards along 20ºW (Fig. 4d-g). The CDOM absorption and fluorescence
261 levels were also generally higher at the southernmost stations due to the impact of the
262 upwelling system of NW Africa, resulting in more CDOM-rich deep waters reaching the
263 surface (Fig. 4 d-g).

264 Vertical profiles were characterised by a subsurface maximum around the depth of the
265 $\overline{\mathrm{N}}$ maximum and the DCM, being shallower for the shorter, $a_{CDOM}(254)$ and $F(280/320)$,
266 than for the longer wavelength, $a_{CDOM}(340)$ and $F(320/410)$, indices. Whereas $a_{CDOM}(254)$
267 varied within a relatively narrow range between 0.98 and 1.75 m^{-1} with a coefficient of
268 variation (C.V.) of 16.1% (Fig. 4d), the variability of $a_{CDOM}(340)$ was much larger: from
269 0.08 to 0.35 m^{-1}, with a C.V. of 40.3% (Fig. 4e). The protein-like fluorescence
270 ($F(280/320)$) varied between 0.43 and 1.98 QSU with a C.V. of 37.8% (Fig. 4f). The
271 fluorescence intensity of the humic-like substances $F(250/435)$ varied between 0.32 and
272 1.23 QSU with a C.V. of 32.4% (data not shown), the terrestrial humic-like substances
273 ($F(340/440)$) between 0.09 and 0.72 QSU with a C.V. of 43.0% (data not shown) and the
274 marine humic-like compounds ($F(320/410)$) between 0.10 and 0.87 QSU with a C.V. of
275 43.7% (Fig. 4f). The three humic-like fluorophores showed similar spatial patterns

276 (F(250/435) vs. F(340/440), $R^2 = 0.97$, n = 62, $p < 0.0001$; F(250/435) vs. F(320/410), R^2
277 $= 0.97$, n = 62, $p < 0.0001$; F(340/440) vs. F(320/410), $R^2 = 0.98$, n = 62, $p < 0.0001$),
278 suggesting that the processes controlling their fluorescence intensities impact them in
279 similar ways.

280 *3.2. Incubation studies conducted in the surface Eastern North Atlantic Ocean*

281 The incubation experiments were conducted at twelve stations (framed stn numbers, Fig.
282 1). Chl *a* concentrations at these sites ranged between 0.11 and 0.19 mg m^{-3}, initial nutrient
283 concentrations were below the detection limit for NH_4^+ and ranged from > 0.1 to 0.6 μmol
284 N l^{-1} for $NO_3^- + NO_2^-$,and from 0.01 to 0.06 μmol P l^{-1} for HPO_4^{2-} (Table 1). Initial DOC
285 concentrations varied between 71 and 83 μmol C l^{-1}. After 72h of incubation, the
286 differences between the initial and final DOC values were < 3 μmol C l^{-1} (data not shown).
287 These changes were not significant considering that the standard error of the determination
288 of DOC was about 1 μmol C l^{-1}. Initial DON (DON_0) concentrations varied between 4.6
289 and 5.4 μmol N l^{-1}, of which 14 ± 9% (average ± SD) was consumed over the 72 hours of
290 incubation (Table 2). The degradation rate of DON, BDON/Δt, varied between 0.09 ± 0.06
291 and 0.48 ± 0.07 μmol N $l^{-1}d^{-1}$ (Table 2). Both the DON_0 and BDON showed generally
292 lower concentrations south of the Azores front region (Fig. 4).

293 Initial bacterial production (BP) rates ranged from 31 ± 14 to 130 ± 46 pmol l^{-1} d^{-1},
294 decreasing by 35 ± 25% (average ± SD) after 72 hours, following the decrease in DON
295 (Table 2 and 3). These BP rates cannot be compared to field measurements because they
296 came from a dilution incubation experiment (more DOM available per bacterial cell) where
297 grazers previously had been eliminated.

298 CDOM absorption coefficients and the fluorescence intensity of *F*(250/435) and
299 *F*(340/440) did not change significantly during the course of the incubations (data not
300 shown). In contrast, *F*(280/320) showed an average decrease of 0.18 ± 0.10 QSU (average
301 ± SD) over the 72 hours incubation period corresponding to 29 ± 9% of the initial
302 fluorescence (Table 2), with a generally lower bioavailability south of the Azores front area
303 (Table 2b; Fig. 4). The consumption of *F*(280/320) followed a first-order kinetics, with an
304 average consumption constant of 9 ± 2 % d^{-1} (Fig. 2a) and a net average decay rate of 0.06
305 ± 0.03 QSU d^{-1} (Table 2b). The initial and bioavailable fraction of *F*(280/320) correlated
306 with each other and both were also significantly correlated with BDON (Eq. 1-2 Table 4;
307 Fig. 5a), while the resistant fraction (R*F*(280/320)) was significantly correlated with initial
308 $a_{CDOM}(254)$, *F*(250/435) and *F*(340/440) (Eq. 3–5 in Table 4). Furthermore, the initial
309 *F*(280/320) was correlated with BDON/Δt (Eq. 6 in Table 4).
310 In our experiments, the *F*(320/410) production followed a first order kinetics, with an
311 average ± SD built-up constant of 7 ± 2 % d^{-1} (Fig. 2b) and a net production rate
312 (P*F*(320/410)/Δt) of 0.013 ± 0.003 QSU d^{-1} (Table 2c; Fig. 2b) resulting in an average
313 increase over the incubation period of 0.04 ± 0.01 QSU (Table 2c). The production of
314 *F*(320/410) reached generally lower levels in the incubations with water collected south of
315 the Azores Front area (Table 2c; Fig.4).
316 The initial *F*(320/410) was significantly correlated with *F*(280/320) and $a_{CDOM}(254)$
317 (Eq. 7–8 in Table 4), while P*F*(320/410) was significantly correlated with BDON and
318 B*F*(280/320) (Eq. 9-10 in Table 4; Fig. 5b), and the R*F*(320/410) was related with
319 R*F*(280/320), $a_{CDOM}(254)$, *F*(250/435) and *F*(340/440) (Eq. 11–14 in Table 4).

320 **4. Discussion**

321 The observed southward increase of salinity and temperature in the upper 200 m has
322 previously been explained by large-scale seasonal heating, evaporation, and advection by
323 the ocean currents crossing the study area (e.g. Pérez et al., 2003; Carracedo et al., 2012).
324 The sharp gradient of the thermohaline properties at about 35°N indicates the presence of
325 the Azores front (Carracedo et al. 2012; Benavides et al., 2013), defined by Pérez et al.
326 (2003) as the position where the 36.2 isoline (Fig. 3a) and 16.2ºC isotherm (Fig. 3b)
327 intercepts 150 m depth. The Azores front, which separates the temperate from the
328 subtropical ENA, is associated to the Azores current, a branch of the Gulf Stream system
329 that originates from near the Grand Banks and flows south-eastwards. It reaches the study
330 area at between 32º and 35°N (Fig. 1), where it can be identified by the strong temperature
331 and salinity gradients (e.g. Péliz et al., 2005). Waters below the seasonal thermocline north
332 of the Azores front corresponded to the subtropical branches of Eastern North Atlantic
333 Central water (ENACW) formed south of 40ºN, which is characterised by temperatures
334 between 12.5 and 16ºC and inorganic nutrient concentrations of 1.2 – 11.1 µmol l^{-1} for
335 NO_3^- and 0.14 – 0.67 µmol l^{-1} for HPO_4^{2-} (Pérez et al., 2003; Ríos et al., 1992; Carracedo
336 et al., 2012; Lønborg and Álvarez-Salgado, 2014). South of the Azores front, the Madeira
337 Mode water (MMW), formed north of the Island of Madeira (Fig. 1), was the dominant
338 water mass below the seasonal thermocline. The MMW is characterised by high salinities
339 of 36.5 – 37.0, temperatures of 18 – 20ºC and NO_3^- and HPO_4^{2-} levels below the detection
340 limit (Pérez et al., 2005; Carracedo et al. 2012; Lønborg and Álvarez-Salgado, 2014).
341 The DOC and DON concentrations measured during the cruise are comparable with
342 previous values reported for surface waters of the North Atlantic (Doval et al. 2001;
343 Carlson et al. 2010; Letscher et al., 2013; Álvarez-Salgado et al., 2013). The highest levels
344 of DOC and DON were observed in the surface 20 m decreasing with depth. DOC

345 increased while DON decreased southwards, which means that the C/N ratio of DOM is
346 higher in the subptropical (~ 12) than in the subpolar ENA (~ 10), coinciding with the
347 lower Chl *a* and higher temperatures and salinities in the Azores front (Fig. 3 & 4). This is
348 consistent with the accumulation of N-poor DOM in subtropical gyres previously described
349 by Hansell et al. (2009). An intrusion of DOM-rich surface water with a high C/N molar
350 ratio of ~12 down to 100 m was found between 35° and 29°N (Fig. 4a, b & c), coinciding
351 with the deepening of the seasonal thermocline (Fig. 3c) characteristic of the subtropical
352 gyre (Doval et al. 2001).

353 The lowest CDOM absorption values were measured south of the Azores front area and
354 in surface waters, while higher values were associated with the DCM. A similar surface
355 distribution and levels has previously been found in both the Atlantic and Pacific Oceans
356 and is linked to the larger impact of CDOM photobleaching in the surface waters and south
357 of the Azores front, and a higher production of CDOM in the DCM area (e.g. Yamashita
358 and Tanoue, 2004; Nelson et al., 2007; Swan et al., 2009). $a_{CDOM}(254)$, a proxy for the
359 abundance of conjugated carbon double bonds (Lakowicz, 2006), showed a lower
360 variability than $a_{CDOM}(340)$ due to photo-bleaching caused by UV-B (280–315 nm) and
361 UV-A (315–400 nm) radiation, suggesting that photo-degradation of aromatic and/or highly
362 complex DOM took place leading to a potential shift of the CDOM absorption towards
363 shorter wavelengths (Blough and Del Vecchio, 2002; Tedetti and Sempéré, 2006; Fichot
364 and Benner, 2011; Helms et al., 2013). In agreement with previous open ocean studies, we
365 also found that the CDOM absorption and DOC concentration did not significantly
366 correlate, suggesting that the processes controlling the distributions of these pools are not
367 directly connected, contrary to coastal waters where a close relationship is typically found

368 mainly due to the large input of coloured terrestrial DOM (Swan et al. 2009; Mendoza and
369 Zika 2014).

370 The vertical distribution of FDOM followed the pattern previously reported for open
371 ocean systems. Generally, FDOM was low in surface waters where sunlight penetrates and
372 photolysis of the coloured DOM compounds takes place, and increasing with depth due to
373 the decreasing impact of photodegradation and increasing impact of microbial processes
374 resulting in a subsurface FDOM maxima (Jørgensen et al., 2011; Stedmon and Álvarez-
375 Salgado 2011; Kowalczuk et al. 2013). The *F*(320/410) and *F*(280/320) levels were
376 generally higher north of the Azores front. These high levels coincided with higher Chl *a*
377 levels, suggesting a link between *F*(320/410) and *F*(280/320) and plankton productivity
378 (Fig. 3d; Fig. 4e & f) as also suggested previously (e.g. Yamashita and Tanoue, 2004;
379 Lønborg and Álvarez-Salgado, 2014). Both the absorption and fluorescence of CDOM
380 showed low levels in the warm waters between 35° and 29°N. The CDOM levels in this area
381 are comparable with previous measurements in the most oligotrophic areas of the ocean and
382 the pattern found is most likely linked to the low productivity of waters carried by Azores
383 Current and following higher penetration of the ultraviolet irradiation leading to an
384 extensive photobleaching during its transport from the origin area near the Grand Banks
385 area towards our study area (Moran et al., 2000; Yamashita and Tanoue 2009; Jørgensen et
386 al., 2011).

387 Differences in the initial DOC and DON concentration and CDOM absorption and
388 fluorescence levels suggested changes in the initial chemical composition of the DOM used
389 for the incubation experiments (Table 1 and 2). Since DOC concentrations did not change
390 significantly over the 72 hours incubation period, we will not discuss these results in more
391 detail. Concerning DON, the consumption of 14 ± 9% (average ± SD) of the initial

392 concentration over the 72 hours of incubation (Table 2) is comparable to estimates
393 previously reported for coastal marine systems (Lønborg and Álvarez-Salgado, 2012).
394 However, Letscher et al. (2013) found that open ocean DON is rather resistant to microbial
395 degradation in surface waters, while it is degraded in the upper mesopelagic zone. The
396 reason for our slightly higher DOM bioavailability in surface waters compared to Letscher
397 et al. (2013), might likely reflect differences in the (1) initial bacterial community
398 composition (Friedline et al., 2012), (2) nutrient conditions (Lønborg and Álvarez-Salgado,
399 2012), (3) variation in DOM chemical composition (Flerus et al., 2012) and/or (4) changes
400 in the impact and magnitude of photochemical processes prior to incubation (Mopper and
401 Kieber, 2002).

402 The fact that the $a_{\mathrm{CDOM}}(254)$, $F(250/435)$ and $F(340/440)$ did not change significantly
403 during the course of the incubations, suggests that these components are of a recalcitrant
404 nature (Yamashita et al., 2008). Conversely, the $F(280/320)$ pool has previously been
405 suggested as a suitable indicator for the dynamics of total hydrolyzable amino acids
406 (THAA) and it could potentially be used to trace the dynamics of the labile DOM pool (e.g.
407 Yamashita and Tanoue, 2003). The $F(280/320)$ showed an average decrease of 29 ± 9%
408 (Table 2), which is similar to values (28 ± 7%) recently reported for the coastal upwelling
409 system of the Ría de Vigo (Lønborg et al., 2010). The $F(280/320)$ consumption followed a
410 first order kinetics, at an average decay rate of 9 ± 3 % d^{-1} (Fig. 2a), which means that
411 these protein-like materials were a limiting factor for bacterial growth and they represented
412 a very labile pool which is used on daily scales (Fig. 2a). This decay rate (9 ± 3 % d^{-1}) is
413 approximately 1/3 of the rates reported (28 ± 13 % d^{-1}) by Lønborg et al. (2010) for the Ría
414 de Vigo, but as this study was conducted in an oligotrophic system with a lower biological
415 production than the Ría de Vigo, a slower decay rate is expected.

416 The relationship between both the initial and the bioavailable *F*(280/320) with BDON,
417 suggests that the protein-like fluorescence could be used to trace the bioavailable DOM
418 components in this open ocean system (Eq. 1 in Table 4; Fig. 5a), but it should be kept in
419 mind that these relationships are unique for this study area and cannot be directly applied to
420 other parts of the oceans. On average, we found that the R*F*(280/320) represented 72 ± 9%
421 of the initial *F*(280/320). We hypothesise that such a large R*F*(280/320) fraction could be
422 due to: i) the fluorescence at *F*(280/320) is due to both labile dissolved free aromatic amino
423 acids and simple peptides as well as amino acid moieties bounded to more complex and
424 recalcitrant structures which are not utilised after 72 h of incubation; and/or ii) co-limitation
425 by inorganic nutrients during the incubation time. In this sense, it should be noted that we
426 have incubated surface ocean waters with average ± SD initial concentrations of inorganic
427 nitrogen and phosphorus of just 0.13 ± 0.17 and 0.03 ± 0.02 µmol l^{-1}, respectively, without
428 any addition of nutrients or organic matter.

429 The marine humic-like fluorescence has previously been suggested as a suitable tracer
430 for recalcitrant DOM, but it has also been shown to be produced as a result of microbial
431 respiration processes (Yamashita and Tanoue, 2004; Castro et al., 2006; Yamashita and
432 Tanoue, 2008; Jørgensen et al, 2011) or the microbial and/or chemical modification of
433 terrestrial humic materials (Andrew et al., 2013). In our incubation experiments with
434 surface waters from the ENA, *F*(320/410) production followed a first order kinetics, with
435 an average ± SD increase of 0.04 ± 0.01 QSU produced at a built-up rate of 7 ± 2 % d^{-1}
436 (Table 2; Fig. 2b), which is comparable to previous estimates (Lønborg et al., 2010). The
437 linear relationships between B*F*(280/320) and BDON with P*F*(320/410) (Eq. 2 and 9 of
438 Table 4; Fig. 5b) also suggests that the bacterial utilization of labile amino acids and DOM
439 is related to the release of refractory humic substances and/or microbially transformed

440 organic matter ending up as recalcitrant DOM, as also suggested by the microbial carbon
441 pump hypothesis (Jiao et al., 2010). The highly significant ($p < 0.002$) positive linear
442 relationship of $a_{CDOM}(254)$, $F(340/440)$ and $F(250/435)$ with R$F(320/410)$ (Eqs. 12–14 of
443 Table 4) suggests that the conjugated carbon double bonds absorbing at 254 nm and the
444 aromatic humic-like rings excited at 250 and 340 nm are of recalcitrant nature. $F(320/410)$
445 has previously been shown to be very sensitive to photo-bleaching by natural solar
446 radiation (Nieto-Cid et al. 2006), so it should be kept in mind that the $F(320/410)$
447 production measured in our dark incubation experiments cannot be directly applied to field
448 conditions. In our experiments, the increase in $F(320/410)$ was not followed by a change in
449 CDOM absorption, suggesting that the humic substances produced by the incubated
450 microbial community were different from those initially present in the sample water. In the
451 water used for the incubation, CDOM could have been produced by viral lysis,
452 phytoplankton release and zooplankton sloppy feeding (Rochelle-Newall and Fisher, 2002;
453 Lønborg et al., 2009; 2013; Romera-Castillo et al., 2010). All these CDOM production
454 pathways were playing no, or only a negligible role in the incubation experiments, leaving
455 microbial transformation as the most likely cause for the observed changes in CDOM.
456 Our field and incubation data allowed us to clearly identify the position of the Azores
457 Front region and couple this to the changes measured in the DON and FDOM pools (Table
458 3; Fig 3a and b). The Azores front region has previously been described as an oligotrophic
459 system with low nutrient and Chl a concentrations, as was also found during the CAIBOX
460 cruise. This study furthermore demonstrates that the levels of BDON, P$F(320/410)$ and
461 *B*F(280/320) are lower south of the Azores Front region, suggesting that the DOM in these
462 waters are of a more recalcitrant nature then found in more productive areas of the open
463 ocean.

464 **5. Conclusions**

465 In this study we combined field and laboratory studies to 1) demonstrate that the
466 coloured and bioavailable fractions of DOM have low levels in the Azores Front area,
467 which is likely due to the extensive photobleaching and low productivity of these waters; 2)
468 show the first quantitative relationships between CDOM fluorescence and DON
469 bioavailability for open ocean surface waters, suggesting that the protein-like fluorescence
470 can be used to trace the bioavailable fraction of DON; and 3) demonstrate that the humic-
471 like fluorophores are produced as a by-product of bacterial metabolism and that they can
472 therefore be used as a proxy for organic matter degradation processes in open ocean
473 systems.

474 **Acknowledgement**

475 We like to thank the captain and crew of R/V Sarmiento de Gamboa and the technicians of
476 the CSIC *Unidad de Tecnologia Marina* (UTM) for their help during the CAIBOX cruise.
477 The collaboration of the chief scientist, M. Gilcoto, and the scientific party on board is also
478 acknowledged. V. Vieitez analysed the inorganic nutrient and M.J. Pazó the DOC/TDN
479 samples. This study was funded by the Spanish Ministry of Science and Innovation, grant
480 CTM2007–66408–C02–01/MAR. C.L. was funded by a Postdoctoral fellowship from the
481 Carlsberg Foundation. GJH was supported by an Austrian Science Fund project (P23234-
482 B11).

483 **References**

484 Álvarez-Salgado, X.A., Nieto–Cid, M., Álvarez, M., Pérez, F.F., Morin, P., Mercier, H.,
485 2013. New insights on the mineralization of dissolved organic matter in central,

486 intermediate and deep water masses of the North–Eastern North Atlantic. Limnol.
487 Oceanogr. 58, 681–696.
488 Andrew, A.A., Del Vecchio, R., Subramaniam, A., Blough, N.V., 2013. Chromophoric
489 dissolved organic matter (CDOM) in the Equatorial Atlantic Ocean: Optical proper-ties
490 and their relation to CDOM structure and source. Mar. Chem. 148: 33-43.
491 Benavides, M., Arístegui J., Agawin, N.S.R., Álvarez-Salgado, X.A., Álvarez, M.,
492 Troupin, C., 2013. Low contribution of N_2 fixation to new production and excess
493 nitrogen in the subtropical northeast Atlantic margin. Deep-Sea Res. I 81, 36–48
494 Blough, N.V., Del Vecchio, R., 2002. Chromophoric DOM in the coastal environment. In:
495 Hansell, D.A., Carlson, C.A. (Eds.), Biogeochemistry of Marine Dissolved organic
496 matter. Academic Press, San Diego, pp. 509–546.
497 Bronk, D.A., 2002. Dynamics of dissolved organic nitrogen. In: Hansell DA, Carlson CA
498 (Eds.) Biogeochemistry of marine dissolved organic matter. Academic Press, USA, p.
499 153–247.
500 Carlson, C.A., Hansell, D.A., Nelson, N.B., Siegel, D.A., Smethie, W.M., Khatiwala, S.,
501 Meyers, M.M., Halewood, E., 2010. Dissolved organic carbon export and subsequent
502 remineralization in the mesopelagic and bathypelagic realms of the North Atlantic basin.
503 Deep-Sea Res. II 57, 1433–1445.
504 Castro, C.G., Nieto-Cid, M., Álvarez-Salgado, X.A., Perez, F.F., 2006. Local
505 remineralization patterns in the mesopelagic zone of the Eastern North Atlantic, off the
506 NW Iberian Peninsula. Deep-Sea Res. I 53, 1925–1940.
507 Coble, P.G., Green, S.A., Blough, N.V., Gasgosian, R.B., 1990. Characterization of
508 dissolved organic matter in the Black Sea by fluorescence spectroscopy. Nature 348,
509 432-435.

510 Coble, P.G., 1996. Characterization of marine and terrestrial DOM in seawater using
511 excitation-emission matrix spectroscopy. Mar. Chem. 51, 325–346.
512 Coble, P.G., 2007. Marine optical biogeochemistry: The chemistry of ocean colour. Chem.
513 Rev. 107, 402–418.
514 Doval, M.D., Álvarez–Salgado, X.A., Pérez, F.F., 2001. Organic matter distributions in the
515 Eastern North Atlantic–Azores Front region. J. Mar. Sys. 30, 33–49
516 Fichot, C. G., Benner, R., 2011. A novel method to estimate DOC concentrations from
517 CDOM absorption coefficients in coastal waters, Geophys. Res.Lett. 38,
518 doi:10.1029/2010GL046152.
519 Flerus, R., Lechtenfeld, O.J., Koch, B.P., McCallister, S.L., Schmitt-Kopplin, P., Benner,
520 R., Kaiser, K., Kattner, G., 2012. A molecular perspective on the ageing of marine
521 dissolved organic matter. Biogeosciences 9, 1935-1955.
522 Friedline, C.J., Franklin, R.B., McCallister, S. L., Rivera, M.C., 2012. Bacterial
523 assemblages of the eastern Atlantic Ocean reveal both vertical and latitudinal
524 biogeographic signatures. Biogeosciences 9, 2177–2193.
525 Guillemette, F., del Giorgio, P.A., 2012. Simultaneous consumption and production of
526 fluorescent dissolved organic matter by lake bacterioplankton. Environ. Micro. 14,
527 1432–1443.
528 Hansen, H.P., Koroleff, F., 1999. Automated chemical analysis. In: Grasshoff, K.,
529 Kermling, K., Ehrhardt, M. (Eds.), Methods of seawater analysis. Wiley-VCH,
530 Germany, pp. 159–226.
531 Hansell, D.A., Carlson, C.A., Repeta, D.J., Schlitzer, R., 2009. Dissolved organic matter in
532 the ocean: New insights stimulated by a controversy. Oceanography 22, 202–211.

533 Hansell, D.A., 2013. Recalcitrant dissolved organic carbon fractions. Annu. Rev. Mar. Sci.
534 5, 421-445.
535 Helms, J.R., Stubbins, A., Perdue, E.M., Green, N.W., Chen, H., Mopper, K., 2013.
536 Photochemical bleaching of oceanic dissolved organic matter and its effect on
537 absorption spectral slope and fluorescence. Mar. Chem. 155, 81–91.
538 Jiao, N., Herndl, G.J., Hansell, D.A., Benner, R., Kattner, G., Wilhelm, S.W., Kirchman,
539 D.L., Weinbauer, M.G., Luo, T., Chen, F., Azam, F., 2010. Microbial production of
540 recalcitrant dissolved organic matter: long-term carbon storage in the global ocean. Nat.
541 Rev. Microbiol. 8, 593–599.
542 Jørgensen, L., Stedmon, C.A., Kragh, T., Markager, S., Middelboe, M., Søndergaard, M.,
543 2011. Global trends in the fluorescence characteristics and distribution of marine
544 dissolved organic matter. Mar. Chem. 126, 139–148.
545 Kirchman, D. L., Suzuki, Y., Garside, C., Ducklow H.W., 1991. High turnover rates of
546 dissolved organic carbon during a spring phytoplankton bloom. Nature 352, 612–614.
547 Kowalczuk, P., Tilstone, G.H., Zabłocka, M., Röttgers, R., Thomas, R. , 2013. Composition
548 of dissolved organic matter along an Atlantic Meridional Transect from fluorescence
549 spectroscopy and Parallel Factor Analysis. Mar. Chem. 157, 170-184
550 Lakowic, J.R., 2006. Principles of Fluorescence Spectroscopy. Springer, Baltimore.
551 Letscher, R., Hansell, D.A. Carlson, C.A., Lumpkin, R., Knapp, A.N., 2013. Dissolved
552 organic nitrogen in the global surface ocean: Distribution and fate. Global Biogeochem.
553 Cycles 27, doi:10.1029/2012GB004449
554 Lønborg C., Álvarez-Salgado, X.A., Davidson, K., Miller, A.E.J., 2009. Production of
555 bioavailable and refractory dissolved organic matter by coastal heterotrophic microbial
556 populations. Estuar. Coast. Shelf Sci. 82, 682–688.

557 Lønborg, C., Álvarez-Salgado, X.A., Davidson, K., Martínez-García, S., Teira, E., 2010.
558 Assessing the microbial bioavailability and degradation rate constants of dissolved
559 organic matter by fluorescence spectroscopy in the coastal upwelling system of the Ría
560 de Vigo. Mar. Chem.119, 121–129.
561 Lønborg, C., Álvarez-Salgado, X.A., 2012. Recycling versus export of bioavailable
562 dissolved organic matter in the coastal ocean and efficiency of the continental shelf
563 pump. Global Biogeochem. Cycles 26, doi:10.1029/2012GB004353.
564 Lønborg, C., Álvarez-Salgado, X.A., 2014. Tracing dissolved organic matter cycling in the
565 eastern boundary of the temperate North Atlantic using absorption and fluorescence
566 spectroscopy. Deep Sea Res. I 85, 35-46.
567 Lønborg, C., Middelboe, M., Brussaard, C.P.D., 2013. Viral lysis of *Micromonas pusilla*:
568 impacts on dissolved organic matter production and composition. Biogeochemistry 116,
569 231–240.
570 Mendoza, W.G., Zika, R.G., 2014. On the temporal variation of DOM fluorescence on the
571 southwest Florida continental shelf. Prog. Ocean. 120, 189–204.
572 Millard, R.C., Owens, W.B., Fofonoff, N.P., 1990. On the calculation of the Brunt- Väisälä
573 frequency. Deep Sea Res. 37, 167-181.
574 Moran, M.A., Sheldon, W.M., Zepp, R.G., 2000. Carbon loss and optical property changes
575 during long-term photochemical and biological degradation of estuarine dissolved
576 organic matter. Limnol. Oceanogr. 45, 1254–1264.
577 Nagata, T., 2000. Production mechanisms of dissolved organic carbon. In: Kirchman DL
578 (ed) Microbial ecology of the oceans, vol 1. Wiley-Liss, New York, pp. 121–153
579 Nelson, N.B., Siegel, D.A., 2013. Global distribution and dynamics of chromophoric
580 dissolved organic matter. Annu. Rev. Mar. Sci. 5, 447–476.

581 Nieto-Cid, M., Álvarez-Salgado, X.A., Pérez, F.F., 2006. Microbial and photochemical
582 reactivity of fluorescent dissolved organic matter in a coastal upwelling system. Limnol.
583 Oceanogr. 51, 1391–1400.
584 Péliz, A., Dubert, J., Santos, A.M.P., Oliveira, P.B., LeCann, B., 2005. Winter upper ocean
585 circulation in the western Iberian basin, fronts, eddies and poleward flows: An overview.
586 Deep-Sea Res. I 52, 621–646.
587 Pérez, F.F., Gilcoto, M., Ríos, A.F., 2003. Large and mesoscale variability of the water
588 masses and the deep chlorophyll maximum in the Azores Front. J. Geophys. Res.-
589 Oceans 108, 3215–3233.
590 Ríos, A.F., Pérez, F.F., Fraga F., 1992. Water masses in the upper and middle North
591 Atlantic Ocean east of the Azores. Deep-Sea Res. 39, 645-658.
592 Rochelle-Newall, E.J., Fisher, T.R., 2002. Production of chromophoric dissolved organic
593 matter fluorescence in marine and estuarine environment: an investigation into the role
594 of phytoplankton. Mar. Chem. 77, 7–21.
595 Romera-Castillo, C., Sarmento, H., Álvarez-Salgado, X.A., Gasol, J.M., Marrasé, C., 2010.
596 Production of chromophoric dissolved organic matter by marine phytoplankton. Limnol.
597 Oceanogr. 55, 446–454.
598 Schlitzer, R. 2012. Ocean Data View 4, http://odv.awi.de
599 Sokal, F.F., Rohlf, F.J., 1995. Biometry. Freeman, New York.
600 Stedmon, C.A., Álvarez-Salgado, X.A., 2011. Shedding light on a black box: UV visible
601 spectroscopic characterization of marine dissolved organic matter. In: Jiao, N., Azam,
602 F., Sanders, S. (Eds.), Microbial carbon pump in the ocean. Science AAA/S, pp. 62–63.
603 Tedetti, M., Sempéré, R., 2006. Penetration of Ultraviolet Radiation in the Marine
604 Environment. A Review. Photochem. Photobiol. 82, 389–397.

605 Yamashita, Y., Tanoue, E., 2003. Chemical characterization of protein-like fluorophores in
606 DOM in relation to aromatic amino acids. Mar. Chem. 82, 255-271.
607 Yamashita, Y., Tanoue, E., 2004. In situ production of chromophoric dissolved organic
608 matter in coastal environments. Geophys. Res. Lett. 31, Doi:10.1029/2004GL019734.
609 Yamashita, Y., Tanoue, E., 2008. Production of bio-refractory fluorescent dissolved
610 organic matter in the ocean interior. Nat. Geosci.1, 579-582.
611 Yamashita, Y, Jaffé, R., Maie, N., Tanoue, E., 2008. Assessing the dynamics of dissolved
612 organic matter (DOM) in coastal environments by excitation emission matrix
613 fluorescence and parallel factor analysis (EEM-PARAFAC). Limnol.Oceanogr.53,
614 1900-1908.
615 Yentsch, C. S., Menzel D. W., 1963. A method for the determination of phytoplankton
616 chlorophyll and phaeophytin by fluorescence, Deep Sea Res. Oceanogr.Abstracts 10,
617 221-231.
618 Yokokawa, T., Sintes, E., De Corte, D., Olbrich, K., Herndl, G.J., 2012. Differentiating
619 leucine incorporation of Archaea and Bacteria throughout the water column of the
620 eastern Atlantic using metabolic inhibitors. Aquat. Microb. Ecol. 66, 247–256.

621 **Figure legends**

622 Fig. 1. Map showing the cruise track on board R/V *Sarmiento de Gamboa* over the period

623 25 July to 14 August 2009. The white dots (○) show the 71 hydrographic stations

624 occupied and the black dots (●) the 16 stations where dissolved organic carbon (DOC)

625 and nitrogen (DON), coloured dissolved organic matter (CDOM) absorption and

626 fluorescence measurements were performed. The framed stations are those where water

627 for the incubation experiments was collected.

628 Fig. 2. Time course of the ratio between the average time point concentration and initial

629 concentration of a) protein-like (F(280/320)) and b) marine humic-like fluorescence

630 (F(320/410)). The dashed lines and error bars represent ± the standard errors.

631 Fig. 3. Contour plots of a) salinity, b) temperature, c) Brunt-Väisälä frequency, d)

632 chlorophyll a (Chl *a*), e) nitrate (NO_3^-) and f) phosphate (HPO_4^{2-}) plotted as a function

633 of depth in meters (y-axis) along the distance of the cruise track starting at stn 1 (x-axis).

634 The solid lines represented in the section plots a) and b) show the 36.2 isohaline and the

635 16.2ºC isotherm respectively. Black dots in e) and f) represent sampling points and the

636 vertical dotted lines mark changes of direction of the cruise track. Images created using

637 Ocean Data View (Schlitzer, 2012).

638 Fig. 4. Contour plots of a) dissolved organic carbon (DOC) and b) nitrogen (DON), c) ratio

639 of DOC to DON (DOC/DON), d) coloured dissolved organic matter (CDOM) absorption

640 coefficient at 254 nm (a_{CDOM}(254)), and e) at 340 nm (a_{CDOM}(340)), f) fluorescence of

641 protein-like (F(280/320)) and g) marine humic-like (F(320/410)) substances plotted as a

642 function of depth in meters (y-axis) along the distance of the cruise track starting at stn 1

643 (x-axis). Black dots represent sampling points and the dotted lines mark changes of

644 direction of the cruise track. Plotting done with Ocean Data View (Schlitzer, 2012).

645 Fig. 5. Plots of the linear relationship between a) bioavailable protein-like fluorescence

646 (B*F*(280/320)) and dissolved organic nitrogen (BDON) and b) the produced marine

647 humic-like fluorescence (P*F*(320/410)) and BDON. Solid lines represent the

648 corresponding regression and the error bars the standard errors. R^2 = coefficient of

649 determination, p = level of significance.

650

651

652 **Table 1.** Biological, chemical and physical properties of the surface (5 m) water samples used for the incubation studies at the

653 time of collection. Salinity, temperature (Temp.), chlorophyll *a* (Chl. *a*), nitrate + nitrite (NO_3^-+NO_2^-) and phosphate (HPO_4^{2-}),

654 CDOM absorption coefficient at 254 ($a_{CDOM}(254)$) and 340 nm ($a_{CDOM}(340)$) and the initial fluorescence intensities of the humic-

655 like fluorophores ($F(250/435)$) and ($F(340/440)$. Standard errors are shown for values which were measured in 4 replicates.

Date	Salinity	Temp. (ºC)	Chl. *a* (mg m^{-3})	NO_3^-+ NO_2^- (μmol l^{-1})	HPO_4^{2-} (μmol l^{-1})	$a_{CDOM}(254)$ (m^{-1})	$a_{CDOM}(340)$ (m^{-1})	$F(250/435)$ (QSU)	$F(340/440)$ (QSU)
26/07/2009	35.7	18.6	0.17	0.6	0.06	1.52 ± 0.04	0.16 ± 0.01	0.83 ± 0.01	0.41 ± 0.01
27/07/2009	35.9	19.7	0.14	0.1	0.02	1.44 ± 0.03	0.12 ± 0.01	0.55 ± 0.03	0.24 ± 0.01
28/07/2009	36.0	19.8	0.14	0.0	0.01	1.42 ± 0.02	0.13 ± 0.01	0.48 ± 0.02	0.18 ± 0.01
29/07/2009	35.9	16.6	0.16	0.1	0.03	1.33 ± 0.01	0.10 ± 0.01	0.45 ± 0.01	0.17 ± 0.03
31/07/2009	35.9	18.9	0.17	0.0	0.03	1.53 ± 0.02	0.15 ± 0.01	0.60 ± 0.03	0.25 ± 0.01
1/08/2009	35.9	19.1	0.19	0.2	0.05	1.51 ± 0.03	0.14 ± 0.01	0.84 ± 0.12	0.37 ± 0.05
3/08/2009	36.3	21.9	0.12	0.1	0.00	1.39 ± 0.02	0.12 ± 0.01	0.43 ± 0.04	0.19 ± 0.01
4/08/2009	36.6	23.2	0.12	0.0	0.02	1.22 ± 0.03	0.06 ± 0.01	0.28 ± 0.03	0.09 ± 0.01
5/08/2009	36.6	23.8	0.11	0.1	0.02	1.26 ± 0.04	0.08 ± 0.01	0.39 ± 0.01	0.13 ± 0.05
7/08/2009	37.0	24.0	0.11	0.1	0.02	1.25 ± 0.03	0.07 ± 0.01	0.39 ± 0.03	0.17 ± 0.01
8/08/2009	37.1	24.0	0.12	0.0	0.03	1.32 ± 0.03	0.09 ± 0.01	0.48 ± 0.02	0.14 ± 0.01
9/08/2009	37.1	23.8	0.12	0.2	0.04	1.36 ± 0.01	0.10 ± 0.01	0.28 ± 0.06	0.09 ± 0.02

656 **Table 2**. Initial (DON(0), *F*(280/320)(0)), final (RDON, R*F*(280/320)) and bioavailable
657 (BDON, B*F*(280/320)) concentrations and degradation rates (BDON/Δt, B*F*(280/320)/Δt) of
658 a) dissolved organic nitrogen (DON) and b) protein-like fluorescence (*F*(280/320)) during
659 the incubation experiments. Table c) shows initial (*F*(320/410)(0)), final (R*F*(320/410)) and
660 produced (P*F*(320/410)) pools of marine humic-like fluorescence (*F*(320/410)) and the
661 production rate (P*F*(320/410)/Δt). Values are averages of 4 replicates ± standard error.

a) Exp.	DON (0) (μmol l^{-1})	RDON (μmol l^{-1})	BDON (μmol l^{-1})	BDON/Δt (μmol l^{-1} d^{-1})
1	5.2 ± 0.2	4.5 ± 0.1	0.7 ± 0.2	0.22 ± 0.07
2	4.7 ± 0.3	3.5 ± 0.1	1.1 ± 0.3	0.38 ± 0.11
3	4.9 ± 0.3	4.3 ± 0.1	0.5 ± 0.3	0.18 ± 0.10
4	5.1 ± 0.4	4.6 ± 0.2	0.5 ± 0.4	0.16 ± 0.14
5	5.0 ± 0.2	3.6 ± 0.1	1.4 ± 0.2	0.48 ± 0.06
6	5.2 ± 0.2	3.8 ± 0.1	1.4 ± 0.2	0.48 ± 0.07
7	4.9 ± 0.4	4.5 ± 0.1	0.5 ± 0.3	0.16 ± 0.13
8	4.9 ± 0.1	3.9 ± 0.2	1.0 ± 0.2	0.34 ± 0.06
9	5.4 ± 0.2	5.1 ± 0.1	0.3 ± 0.2	0.09 ± 0.06
10	5.4 ± 0.2	5.1 ± 0.1	0.4 ± 0.2	0.12 ± 0.08
11	4.6 ± 0.3	4.3 ± 0.2	0.3 ± 0.3	0.09 ± 0.08
12	5.4 ± 0.2	4.9 ± 0.1	0.5 ± 0.2	0.18 ± 0.06

b) Exp.	*F*(280/320)(0) (QSU)	R*F*(280/320) (QSU)	B*F*(280/320) (QSU)	B*F*(280/320)/Δt (QSU d^{-1})
1	0.65 ± 0.01	0.51 ± 0.05	0.14 ± 0.05	0.048 ± 0.016
2	0.79 ± 0.01	0.50 ± 0.02	0.29 ± 0.02	0.097 ± 0.008
3	0.51 ± 0.01	0.41 ± 0.02	0.10 ± 0.02	0.032 ± 0.008
4	0.59 ± 0.01	0.42 ± 0.01	0.17 ± 0.01	0.056 ± 0.003
5	0.83 ± 0.05	0.49 ± 0.03	0.35 ± 0.05	0.115 ± 0.018
6	0.85 ± 0.01	0.53 ± 0.01	0.33 ± 0.02	0.109 ± 0.006
7	0.48 ± 0.01	0.37 ± 0.01	0.10 ± 0.01	0.034 ± 0.003
8	0.57 ± 0.01	0.35 ± 0.02	0.22 ± 0.02	0.073 ± 0.006
9	0.43 ± 0.01	0.33 ± 0.01	0.09 ± 0.01	0.031 ± 0.002
10	0.43 ± 0.02	0.36 ± 0.01	0.07 ± 0.02	0.023 ± 0.006
11	0.40 ± 0.01	0.31 ± 0.01	0.09 ± 0.01	0.031 ± 0.005

12	0.53 ± 0.01	0.35 ± 0.01	0.18 ± 0.01	0.060 ± 0.004

c) Exp.	*F*(320/410)(0) (QSU)	R*F*(320/410) (QSU)	P*F*(320/410) (QSU)	P*F*(320/410)/Δt (QSU d^{-1})
1	0.43 ± 0.01	0.47 ± 0.01	0.04 ± 0.01	0.013 ± 0.001
2	0.31 ± 0.01	0.36 ± 0.01	0.05 ± 0.01	0.018 ± 0.003
3	0.23 ± 0.01	0.27 ± 0.01	0.04 ± 0.01	0.013 ± 0.004
4	0.24 ± 0.01	0.28 ± 0.01	0.05 ± 0.01	0.015 ± 0.005
5	0.34 ± 0.01	0.40 ± 0.01	0.06 ± 0.01	0.020± 0.002
6	0.33 ± 0.01	0.37 ± 0.01	0.05 ± 0.01	0.015 ± 0.002
7	0.16 ± 0.01	0.20 ± 0.01	0.04 ± 0.01	0.014 ± 0.002
8	0.12 ± 0.01	0.16 ± 0.01	0.03 ± 0.01	0.011 ± 0.004
9	0.12 ± 0.01	0.14 ± 0.01	0.03 ± 0.01	0.009 ± 0.001
10	0.13 ± 0.01	0.16 ± 0.01	0.03 ± 0.01	0.011 ± 0.002
11	0.12 ± 0.01	0.15 ± 0.01	0.03 ± 0.01	0.011 ± 0.002
12	0.11 ± 0.01	0.14 ± 0.01	0.03 ± 0.01	0.010 ± 0.002

662

663

664 **Table 3.** Leucine incorporation rates of the bacterial community at times 0 (BP (0)) and 72

665 hours (BP (72)) of incubation. Values are averages of 2 replicates ± standard error, n.d. =

666 not determined.

Exp.	BP (0) (pmol l^{-1} d^{-1})	BP (72) (pmol l^{-1} d^{-1})
1	89 ± 16	66 ± 6
2	73 ± 6	58 ± 27
3	69 ± 14	56 ± 3
4	130 ± 36	69 ± 1
5	101 ± 4	n.d.
6	114 ± 41	50 ± 16
7	83 ± 2	19 ± 1
8	83 ± 6	26 ± 3
9	96 ± 1	75 ± 7
10	31 ± 14	35 ± 1
11	47 ± 26	40 ± 1
12	75 ± 2	69 ± 2

667

668

669 **Table 4.** Significant linear regressions between bioavailable dissolved organic nitrogen

670 (BDON), absorption coefficient of CDOM at 254 nm (a_{CDOM}(254)), initial (*F*(280/320)(0),

671 *F*(320/410)(0), *F*(250/435)(0) and *F*(340/440) (0)), bioavailable (B*F*(280/320)), produced

672 (P*F*(320/410)) and recalcitrant (R*F*(280/320) and R*F*(320/410)) protein- and humic-like

673 fluorescence, bioavailable protein-like (B*F*(280/320) and produced humic-like fluorescence

674 (P*F*(320/410)), and the degradation rate of BDON (BDON/Δt). Slope, intercept, and

675 standard error (SE) are values found by Model II regression. R^2 = coefficient of

676 determination, p = level of significance, n.s. - not significant.

Eq No.	X	Y	Slope (±SE)	Intercept (±SE)	R^2	p
1	*F*(280/320)(0)	BDON	2.6 ± 0.3	–0.84 ± 0.18	0.90	<0.0001
2	B*F*(280/320)	BDON	4.1 ± 0.4	n.s.	0.91	<0.0001
3	R*F*(280/320)	a_{CDOM}(254)	1.4 ± 0.3	0.78 ± 0.10	0.72	<0.0002
4	R*F*(280/320)	*F*(250/435)(0)	1.2 ± 0.5	n.s.	0.70	< 0.001
5	RF(280/320)	*F*(340/440)(0)	1.4 ± 0.3	–0.37 ± 0.09	0.74	< 0.001
6	*F*(280/320)(0)	BDON/Δt	0.41 ± 0.17	n.s.	0.62	<0.003
7	*F*(320/410)(0)	*F*(280/320)(0)	1.75± 0.4	0.27 ± 0.01	0.63	<0.003
8	*F*(320/410)(0)	a_{CDOM}(254)	0.98 ± 0.17	1.15 ± 0.04	0.76	<0.002
9	P*F*(320/410)	BDON	45 ± 14	- 1.1 ± 0.4	0.52	<0.008
10	P*F*(320/410)	*BF*(280/320)	4.4 ± 2.5	n.s.	0.62	<0.003
11	R*F*(320/410)	RF(280/320)	0.65 ± 0.06	0.38 ± 0.02	0.91	<0.0001
12	R*F*(320/410)	a_{CDOM}(254)	0.92 ± 0.16	1.36 ± 0.04	0.77	<0.002
13	R*F*(320/410)	*F*(250/435)(0)	1.6 ± 0.3	0.41 ± 0.07	0.76	<0.0003
14	R*F*(320/410)	*F*(340/440)(0)	0.87 ± 0.14	0.15 ± 0.04	0.79	<0.0001

677

678

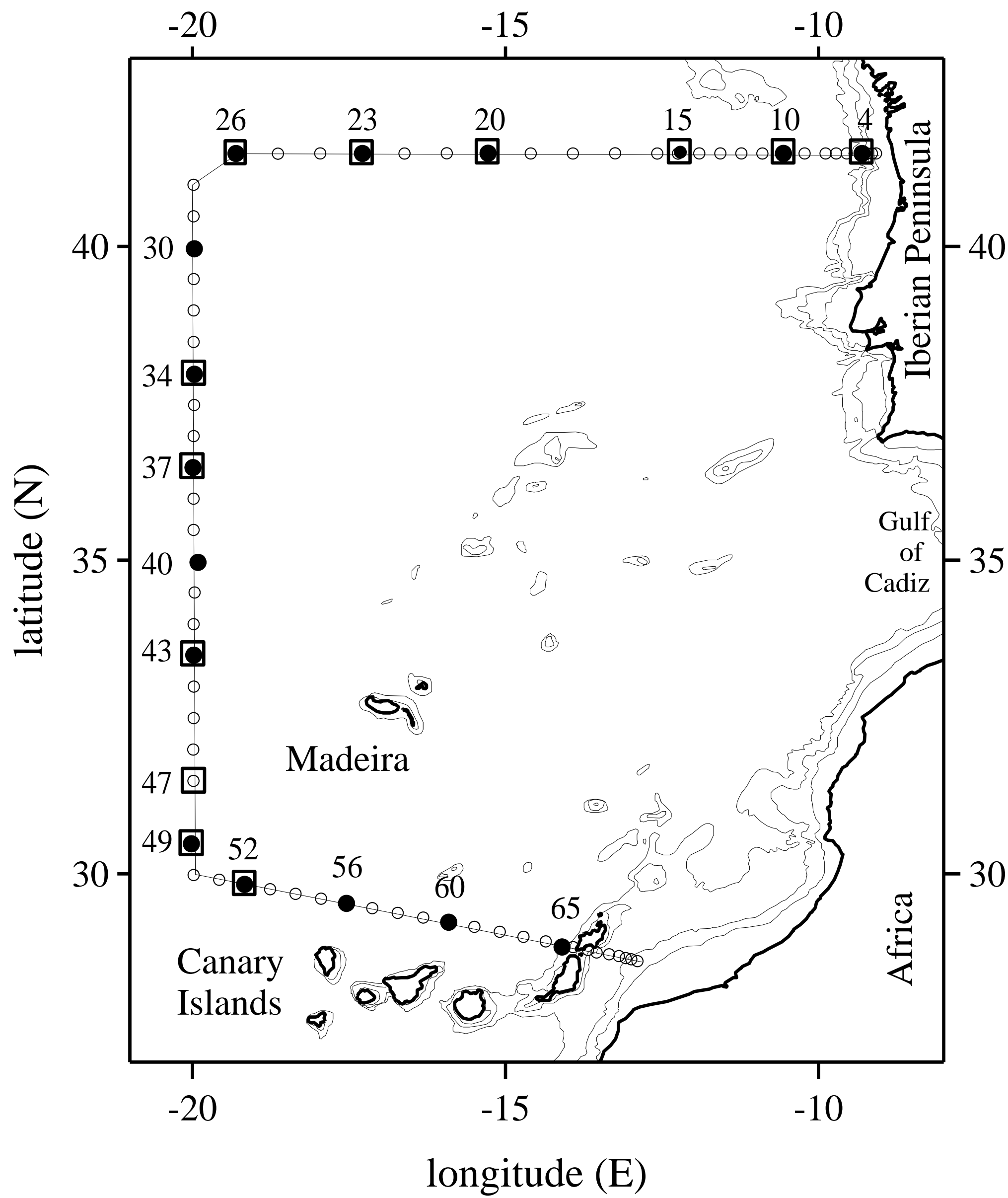

679

680 Lønborg et al., Fig. 1

681

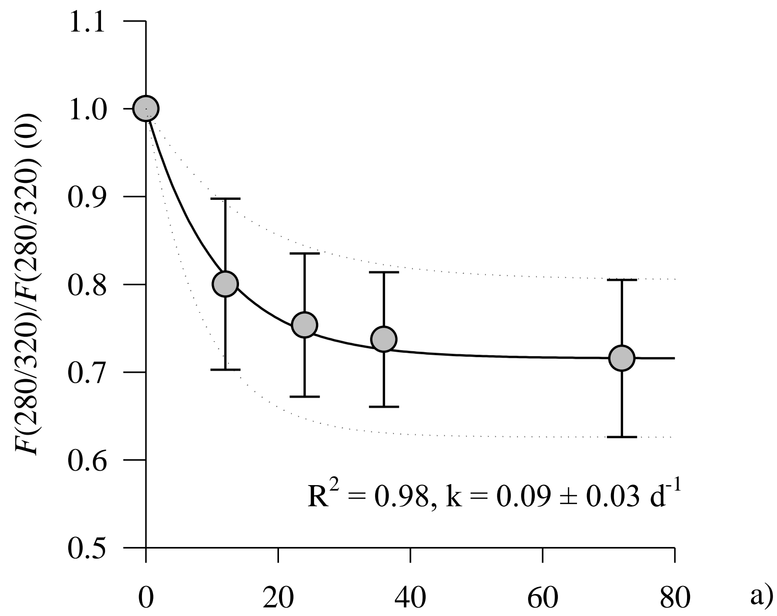

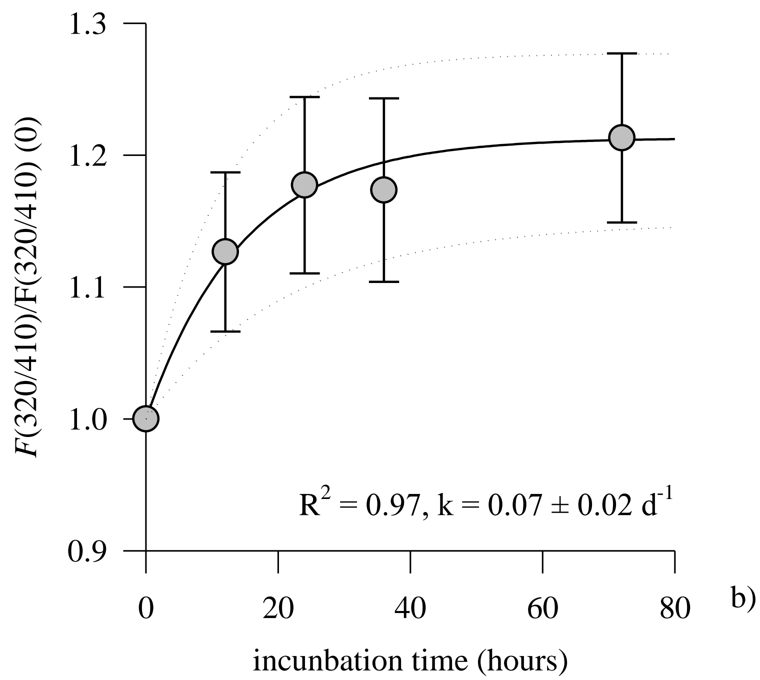

682

683 Lønborg et al., Fig. 2

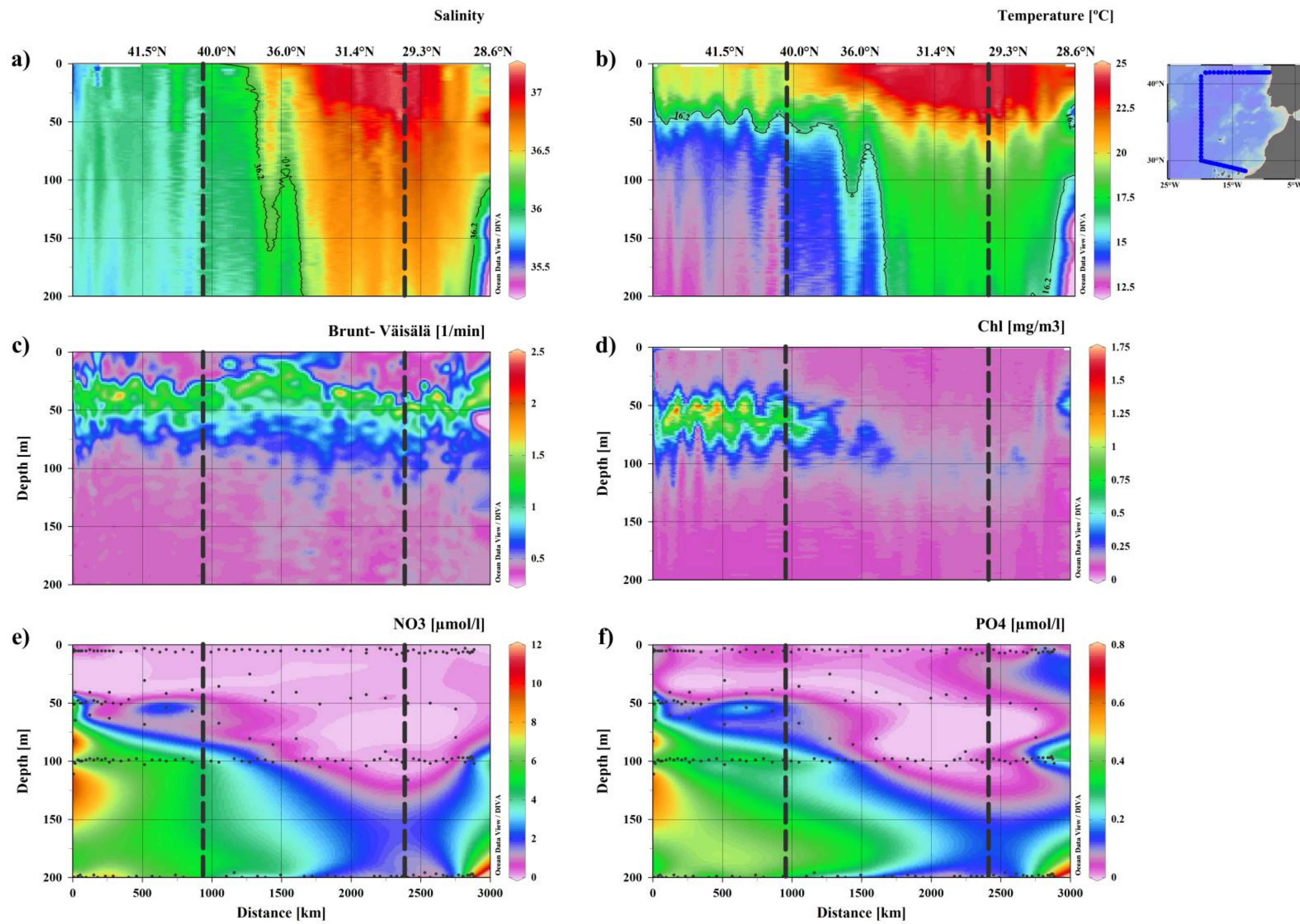

684

685 Lønborg et al., Fig. 3

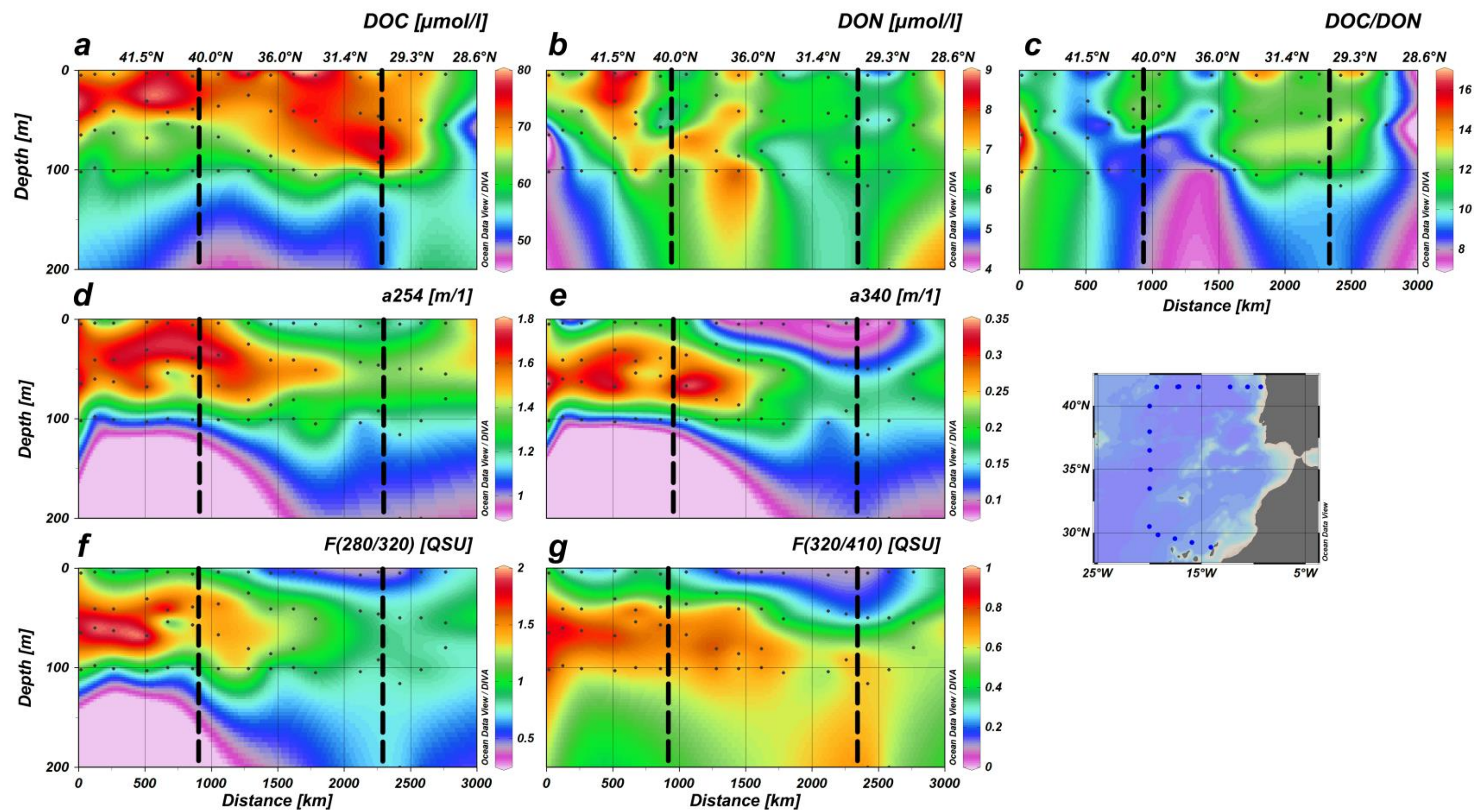

686

687 Lønborg et al., Fig. 4.

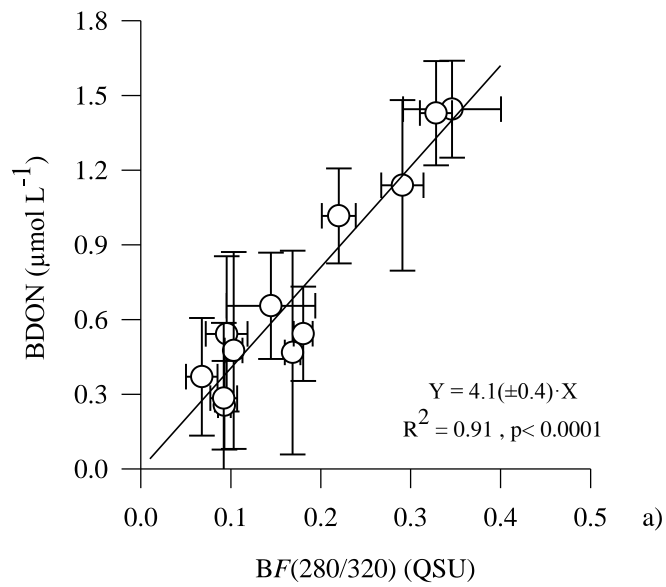

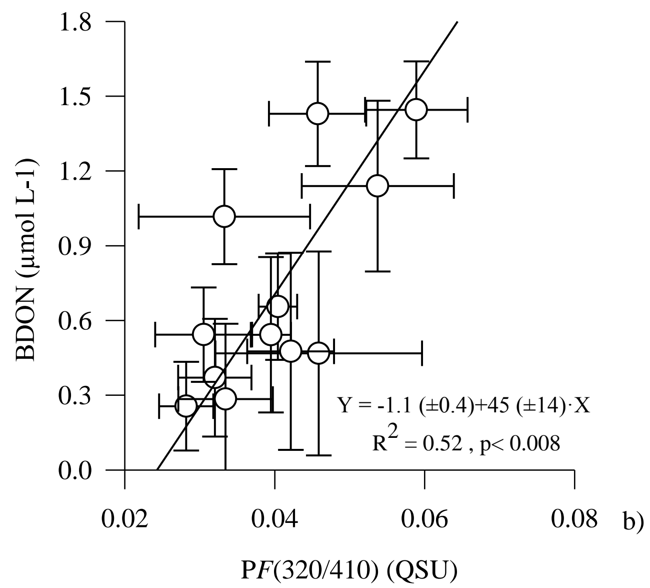

688

689 Lønborg et al., Fig. 5.